Doppler Enhanced Frontal Radar Images of Multiple Human Activities

Shobha Sundar Ram Dept. of Electronics and Communication
Indraprastha Institute of Information Technology
New Delhi, India - 110020
Email: shobha@iiitd.ac.in

***Abstract*—Current through-wall radar implementations yield top-view images of human activities. However, radar operators may find frontal images of humans easier to interpret since they resemble human perspectives. High-resolution frontal images are challenging to generate since they require large radar apertures and high carrier frequencies. We propose a methodology to generate high-resolution frontal images of moving humans using a Doppler radar with a limited size aperture operating at a low carrier frequency. The target is imaged using three dimensional Fourier processing along azimuth, elevation and Doppler. The additional Doppler dimension enables us to reduce the resolution requirements along the cross-range dimensions in terms of aperture size and number of elements. Additionally, we analyze the effect of Doppler resolution, the orientation and range of the human subject with respect to the radar for three different human activities - running, skipping and crawling.**

I. Introduction

Over the last decade, both narrowband and wideband radars have been developed for through-wall imaging of human activities [1]–[6]. Wideband waveforms are particularly useful for generating top-view (range and cross-range) images of humans. However, very large bandwidths are required since humans are usually narrow along the down-range dimension. Large bandwidths are challenging to implement, especially at the low carrier frequencies required for through-wall penetration. Also, top-view images are not very informative regarding the nature of the human activity. In comparison, front-view radar images of humans may convey far more information to a radar operator since they resemble human perspectives more closely. However, frontal images are also difficult to generate. For example, if we wish to resolve 10×10 point scatterers across a human of $1.5m \times 1.5m$ size at a distance of 10m from a radar operating at λ wavelength, we would require a radar aperture that is approximately $\frac{100\lambda}{1.5} \times \frac{100\lambda}{1.5}$. As the resolution requirements of the image increase i.e. if we wish to resolve a greater number of point scatterers, then the size of the aperture becomes fairly large especially at low carrier frequencies. If the radar must have beam scanning capability as well, the elements must be closely space. This results in a costly and complex radar system with a large number antenna elements and associated data acquisition circuitry. In this paper, we propose using Doppler information of moving humans to generate frontal radar images of human activities with reduced radar aperture sizes (and correspondingly, reduced array elements).

Doppler data of moving humans have been exploited for identifying and classifying different types of human motions [7]–[12]. The performance of these classification algorithms, however, depend on the availability of large training databases across different data collection paradigms. Such a training database can be difficult to generate since human motions are often unpredictable especially in law enforcement scenarios. We propose to use Doppler data in a different way. Since humans are non-rigid targets, the different body parts often move at distinct velocities and hence can be resolved on the basis of their unique Doppler. In [13], Doppler data of humans were exploited towards generating frontal images of humans using a very low complexity radar with just three antenna elements arranged in an L shaped configuration. Multiple point scatterers were first resolved on the basis of their Doppler. Then the azimuth and elevation of each of the distinct scatterers were determined using two-element interferometry. However, the quality of the frontal images from this low complexity radar is poor when there is overlap of the Dopplers of the different moving parts. In [14], we proposed using a Doppler radar with a multiple element uniform planar array. The multiple point scatterers on the human body were resolved on the basis of unique Doppler, azimuth and elevation. The additional Doppler dimension allowed us to reduce the resolution requirements in terms of aperture size and number of elements along the two cross-range dimensions. In [14], the methodology involving three-dimensional Fourier processing were restricted to simple walking motion of a human in a straight path towards the radar. In this paper, we study the robustness of the methodology to different complex motions such as running, crawling and skipping. We also investigate the effect of the range and orientation of the human target with respect to the radar.

Our paper is organized as follows. In section II, we present the methodology to generate frontal images of humans using three-dimensional Fourier processing in the Doppler, azimuth and elevation dimensions. In section III, we present frontal images of three different human activities, running, crawling and skipping, from simulated Doppler radar data. We analyze the impact of target's range, orientation and micro-Doppler, with respect to the radar, on the image quality.

II. Doppler Enhanced Imaging with Three Dimensional Fourier Processing

Consider a continuous wave Doppler radar system with a single transmitter and $M \times N$ receiver elements configured as a

978-1-4799-8232-5/151$31.00@2015IEEE

uniform planar array in the $Y-Z$ plane. Assume that the target consists of multiple point scatterers located at (r_b, θ_b, ϕ_b), each moving with a radial velocity v_b with respect to the radar. Therefore, the time domain scattered radar returns at each $(m,n)^{th}$ element is given by

$$y(m,n,t) = \sum_b a_b e^{-jk(r_b - d(m-1)\cos\theta_b \sin\phi_b - d(n-1)\sin\theta_b - 2v_b t)} \quad (1)$$

Here, a_b is the magnitude of the scattered signal from each point scatterer of the target, d is the spacing between adjacent receiver elements and $k = \frac{2\pi}{\lambda}$ is the propagation vector. a_b includes the transmission propagation vector and the reflection from the point scatterer on the human body. Two dimensional Fourier transform along the spatial dimensions, for every time instant, results in $\chi_{2D} = \sum_b a_b H_{2D}[\sin\theta - \sin\theta_b, \sin\phi - \sin\phi_b, t]$. The spatial resolution in the two-dimensional space is inversely proportional to $\frac{r_b\lambda}{Nd} \times \frac{r_b\lambda}{Md}$ i.e. the radar aperture size. Therefore, the spatial resolution can be improved by either increasing the number of elements or by reducing the wavelength. However, the size, cost and complexity of the radar will significantly increase when the number of elements are increased; and high carrier frequencies are unsuitable for through-wall imaging purposes since most building materials significantly attenuate frequencies above the X band.

In order to improve upon the spatial resolution limits without changing the radar parameters, we propose to implement three-dimensional Fourier processing across azimuth, elevation and Doppler dimensions on the radar data. Since humans are dynamic targets, the velocity of the different point scatterers do not remain constant with time. Therefore, we use the short-time Fourier transform across the time domain to represent the data in the joint time-frequency space. This results in $\chi_{3D} = \sum_b a_b H_{3D}[\sin\theta - \sin\theta_b, \sin\phi - \sin\phi_b, f - f_D, t]$. The Doppler ambiguity is inversely proportional to the dwell time of the STFT operation. χ_{3D} is projected to the conventional two-dimensional azimuth-elevation space through two steps. First, we identify the peak scatterers corresponding to each Doppler in χ_{3D};

$$a_p(f) = max_{\theta_p,\phi_p} |\chi_{3D}(\theta, \phi, f)| \quad (2)$$

Second, we convolve each peak scatterer with strength a_p and position (θ_p, ϕ_p) with a point spread function, $h_{small}(\theta, \phi)$, in azimuth-elevation space and sum the resulting responses.

$$\tilde{\chi}_{2D} = \sum_f a_p(f) h_{small}(\theta - \theta_p, \phi - \phi_p) \quad (3)$$

Note that h_{small} is chosen to be of much smaller azimuth and elevation ambiguity in the 2-D space compared to $H_{2D}(\theta, \phi)$ which is governed by the radar aperture size. The resulting image, $\tilde{\chi}_{2D}$, differs from χ_{2D} in multiple ways:

- Since, this algorithm involves an additional Doppler processing step, the resolution requirements in the azimuth-elevation space are reduced.
- When the Doppler, azimuth and elevation ambiguities corresponding to different point scatterers overlap, the performance of the algorithm will degrade.
- $\tilde{\chi}_{2D}$, is generated from the averaged motion of the point scatterers across the short time window. If the velocity and the position of the point scatterer change significantly during the short time duration, then there may be some blurring in the image.
- The algorithm can only be used to image those body parts that are moving. Hence, it is suitable only for imaging regularized motions of the human such as walking, running, crawling, skipping etc. The algorithm is not suited to image motions such as a human standing still and waving his hand.

Cases	Range (m)	Azimuth (°)	Elevation (°)	Doppler (Hz)
1	[10,10]	[0,5]	[30,30]	[40,25]
2	[30,30]	[0,5]	[30,30]	[40,25]
3	[10,10]	[0,5]	[30,30]	[40,35]

TABLE I
CHARACTERISTICS OF A COMPLEX TARGET WITH TWO POINT SCATTERERS

To illustrate the above method, we consider a complex target with two point scatterers with parameters as shown in case.1 of Table.I. Fig.1(a) shows the image of the target generated with two-dimensional array processing of data obtained from 20×20 elements at a carrier frequency of 7.5GHz . The elements are assumed to be spaced half wavelength apart. The image is shown in the polar format as a function of the elevation and azimuth. The image is clearly characterized by poor spatial resolution as we are unable to distinguish two distinct point scatterers. One possible method to improve the image quality is to increase the aperture size or carrier frequency. Instead, we implement Doppler processing in conjunction with array processing as described earlier. We use a short time window of 0.5s while implementing STFT. The resulting image, $\tilde{\chi}_{2D}$, is shown in Fig1(b). Despite retaining the same radar parameters (aperture size and carrier frequency), we are able to clearly distinguish both the point scatterers. Next, we study how the range and orientation of the target with respect to the radar impact the performance of the algorithm. We consider case 2 and case 3 of Table.I. When the two point scatterers are further away from the radar, the spatial resolution degrades as seen in Fig.1(c). However, we are still able to distinguish the two targets. When we consider two point scatterers with similar range but overlap in the Doppler ambiguity (which is inversely proportional to the short time window), the image in Fig.1(d) has significantly degraded. Therefore, when the point scatterers move in orientations that result in very low Dopplers (for example - tangential direction), or when the Dopplers overlap due to similar velocities, the performance of the algorithm begins to deteriorate.

III. EXPERIMENTAL RESULTS FOR SIMULATED HUMAN RADAR DATA

In this section, we will apply the algorithm described in the previous section on simulated Doppler radar data of humans. We consider three human activities - running, skipping and crawling, from ACCAD Carnegie Mellon University's motion capture database. We simulate the data by combining these computer animation data with primitive based electromagnetic

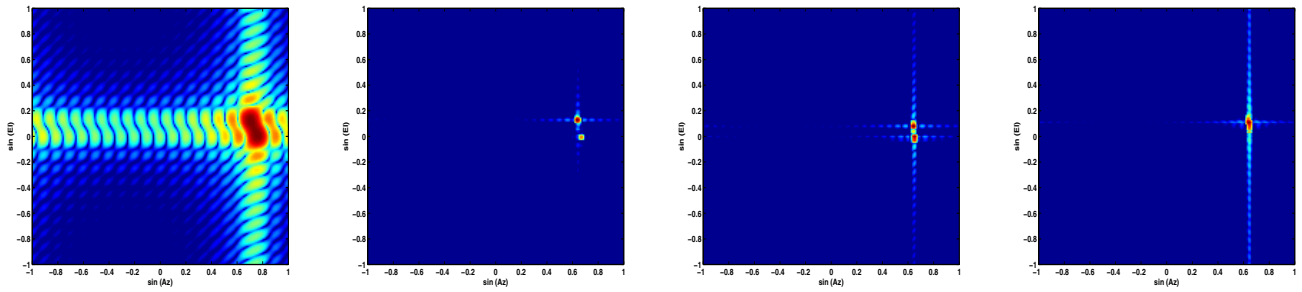

(a) (b) (c) (d)

Fig. 1. Radar image of two point targets generated by (a) two-dimensional array processing (azimuth and elevation) and (b) three-dimensional Fourier processing (Doppler, azimuth and elevation) when target characteristics are as specified in case 1 of Table.I; . Doppler-enhanced radar image when target characteristics are as specified (c) in case 2 of Table.I and (d) in case 3 of Table.I.

modeling [15]. In all three cases, we assume that the radar consists of a single transmitter operating at 7.5GHz and a $[20 \times 20]$ receiver array where the elements are spaced half-wavelength apart. For each case, we consider two types of radar configurations - Radar1 and Radar2. Radar1 is configured such that the receiver array is normal to the direction of translational motion of the human. Therefore most micro-Dopplers are high due to the radial motion of the body parts. Radar2 is configured such that the receiver array is parallel to the direction of the human motion. Therefore, some micro-Dopplers may be low due to the tangential motion of the body parts with respect to the radar.

A. Case 1: Running

First, we consider the running motion. The human is 1.5m tall and 0.5m wide. He runs from $[-3, 1, -3]m$ to $[+3, 1, +3]m$ over $1.53s$ as shown in Fig.2(a). The positions correspond to the ceter of gravity of the human at the hip. The radar is assumed to operate at 7.5GHz and the data are simulated at a sampling frequency of 1400Hz, based on Nyquist conditions for two different planar array configurations (Radar1 and Radar2). Radar1's aperture is aligned normally to the direction of the human motion and centered at $[4, 1, 4]m$. The inset in Fig.2(a) corresponding to this position of the radar shows the perspective of the human seen by the radar at one time frame ($t = 0.67s$). At this instant, the human is $10m$ from the radar. The human consists of multiple point scatterers corresponding to different body parts. Fig.2(b) shows the image, χ_{2D}, generated through two-dimensional array processing along the azimuth-elevation axis. The image is characterized by poor spatial resolution even with the large number of radar elements (400). Further increase of the size of the aperture to $[150 \times 150]$ elements gives rise to an image (not shown here) with adequate spatial resolution (especially along the azimuth dimension). It becomes fairly obvious that such a radar system would be much too costly and complex to be practically viable. Therefore, we implement to introduce the Doppler processing step, as proposed by this paper, to generate a high resolution image without changing the radar parameters (i.e. 400 radar elements operating at 7.5GHz). A short time window of 0.1s was selected to optimize for both time and frequency resolutions in the joint time-frequency space. The spectrogram generated from a single sensor data is shown in Fig.2(c). Since most of the motions are radial with respect to the radar, the Dopplers of the different point scatterers are high. The figure clearly shows that Doppler tracks from different body parts are well resolved at some time instants (like $0.67s$) and significantly overlap at others ($0.55s$). Fig.2(d) shows the frontal image of the human generated through Doppler and array processing at $0.67s$. The figure shows qualitative resemblance to the frontal perspective presented in the inset in Fig.2(a). In this image, we can clearly distinguish the head, the two arms, two legs and the torso of the human. The image quality is significantly poorer when the Dopplers are low at $0.55s$ (figure not shown here). Similarly, when the human is further away from the radar at a distance of $15m$, the spatial resolution slightly degrades with the increase in range resulting in a degradation of the image quality (figure is not shown here). Next, we consider a different orientation of the human with respect to the radar. Radar2's 2D aperture is parallel to the translational motion of human and centered at $[-3, 1, 3]m$ as shown in Fig.2(a). Fig.2(e) shows the image of the human generated from two-dimensional array processing at $0.67s$. Again, the image is characterized by poor spatial resolution which can be improved only by increasing the aperture size or by reducing the carrier frequency. Fig.2(f) shows the spectrogram generated from the time-domain data from a single sensor. The Doppler is initially positive as the human approaches the radar and then is negative as he moves away from the radar. The Doppler tracks from different body parts are not as well resolved as Fig.2(c) since several motions are tangential with respect to the radar. Also, note from the inset in Fig.2(a), the different point scatterers on the arms and legs considerably overlap along the azimuth. Fig.2(g) shows the image of the human generated from three-dimensional Fourier processing along Doppler, azimuth and elevation. Though we can distinguish some parts of the human (legs and one arm), the image is considerably distorted. This can be attributed to considerable overlap of the Doppler and azimuth ambiguities at this orientation.

B. Case 2: Skipping

Next, we consider a human skipping motion. He moves from $[-3, 1, 3]m$ to $[3, 1, -3]m$ along a straight line in $3.8s$ as

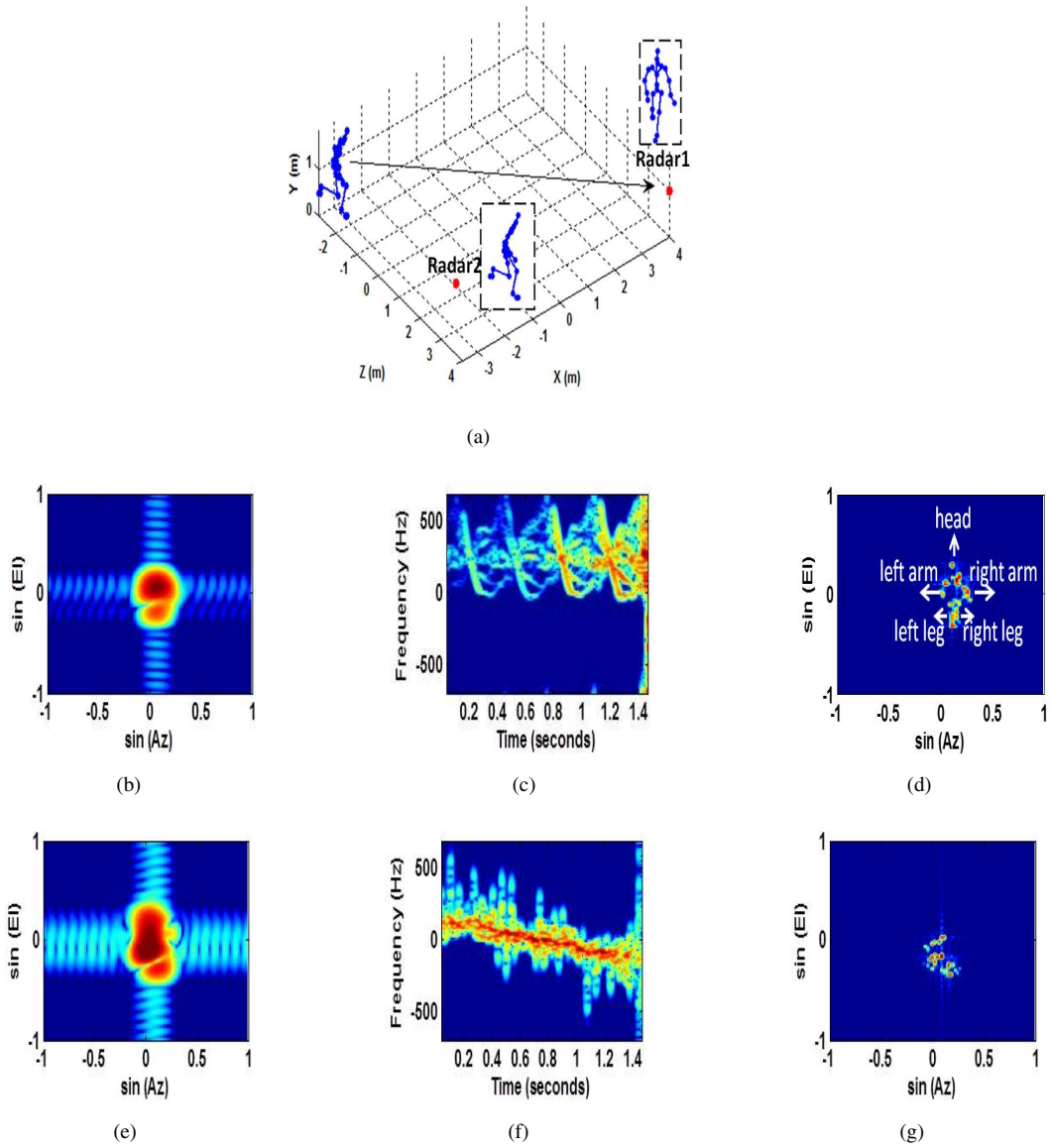

Fig. 2. (a) Animation model of a running human for two radar configurations; Radar1 corresponds to an aperture perpendicular to the translational motion; Radar2 corresponds to an aperture parallel to the translational motion. (b) and (e) are frontal images of the human generated by two-dimensional array processing; (c) and (f) are Doppler spectrograms generated from time-domain data from a single sensor element; (d) and (g) are Doppler-enhanced frontal images of the human generated by three-dimensional Fourier processing - for Radar1 and Radar2 respectively.

shown in Fig.3(a). While skipping, there is a bobbing motion of the entire body along the vertical direction. The data is simulated at a sampling frequency of 600Hz for two different radar configurations. First, we assume that Radar1, centered at $[4, 1, -4]m$, is normal with respect to the human motion. Fig.3(b) shows the 2D image of the human generated from beamforming of the scattered returns at $2.4s$. Even with 400 elements, the spatial resolution is quite poor and we are unable to retrieve a meaningful image of the human. Therefore, we introduce an additional Doppler processing step. The joint time-frequency spectrogram of time domain data from a single sensor is shown in Fig.3(c). A short time window of $0.1s$ is used. The micro-Doppler features in the spectrogram are quite distinct from those of the running motion. There are several instances when the micro-Dopplers are well resolved such as $0.75s$, $1.6s$ and $2.4s$. Fig.3(d) shows the Doppler-enhanced radar image of the human at $2.4s$. This image is considerably similar to the inset in Fig.3(a) corresponding to the frontal perspective of the human from the radar at $[4, 1, -4]m$. We are clearly able to discern some parts of the human. When multiple frames are generated and viewed, we can clearly discern the skipping motion. The head of the human rises and falls as he skips. Next, we consider Radar2 centered at $[3, 1, 3]m$ (shown in Fig.3(a)). The Doppler spectrogram generated from data at a single element is shown in Fig.3(e). Note that some of the micro-Doppler components are quite high even at this orientation at $2.4s$. We generate the frontal image of the human at this orientation using three-dimensional Fourier processing (Doppler, azimuth and elevation) instead of the regular two-dimensional beamforming at $2.4s$. We are

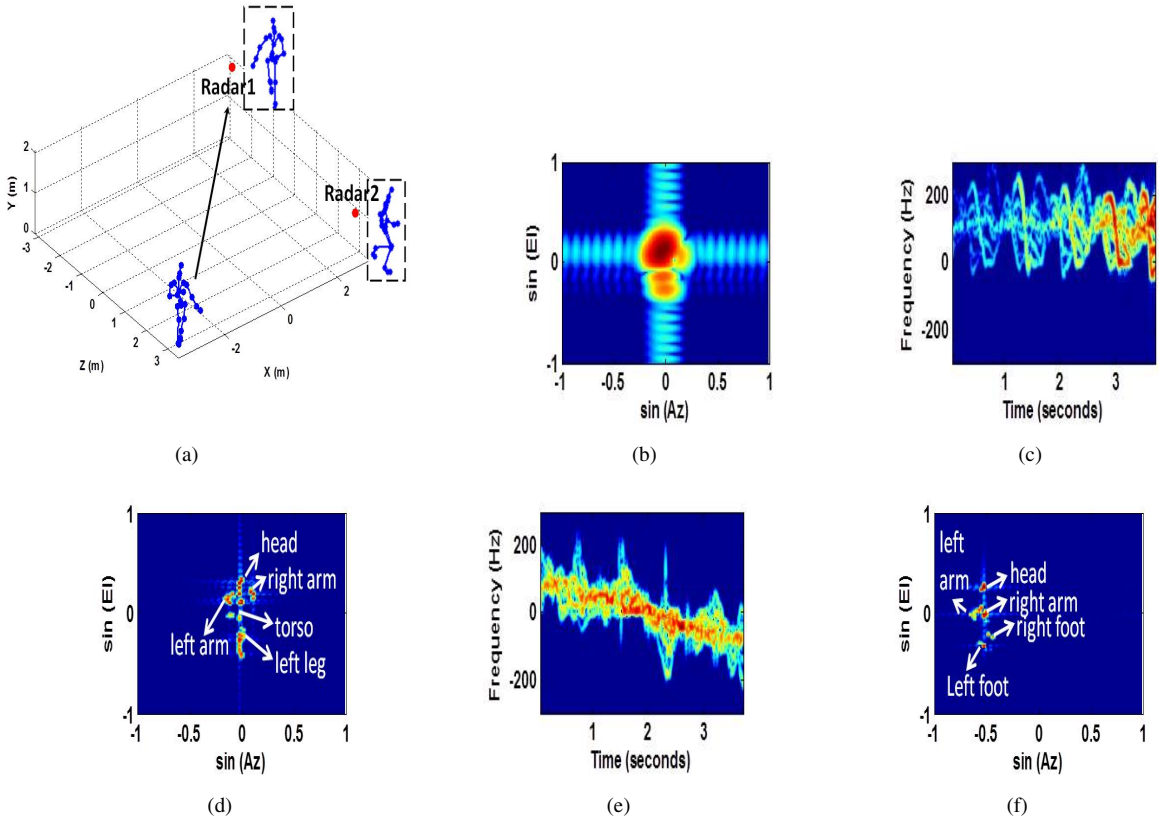

(a) (b) (c) (d) (e) (f)

Fig. 3. (a) Animation model of a skipping human for two radar configurations: Radar1 corresponds to an aperture perpendicular to the translational motion; Radar2 corresponds to an aperture parallel to the translational motion. (b) is the frontal image of the human generated by two-dimensional array processing of data received at Radar1; (c) and (e) are Doppler spectrograms generated from time-domain data from a single sensor element; (d) and (f) are Doppler-enhanced frontal images of the human generated by three-dimensional Fourier processing - for Radar1 and Radar2 respectively.

able to discern the side-view of the human in Fig.3(f). This compares reasonably with the frontal perspective of the human from this target orientation, shown in the inset in Fig.3(a). The improvements in the performance of the imaging of skipping motion in comparison to the previous results from the running motion are due to the reduced overlap of Doppler, azimuth and elevation ambiguities of this motion.

C. Case 3: Crawling

Finally, we consider a third case where the human is crawling (in a soldier fashion) as shown in Fig.4(a). The human moves along a straight path from $[2, 0.25, 1]m$ to $[-4, 0.25, 1]m$ in $10.7s$. Here, Radar1 is centered at $[-5, 1, 1]m$. Therefore, the human is moving mostly radially towards the radar. Fig.4(b) shows the spectrogram of the crawling motion. The micro-Doppler signature of the crawling motion is characterized by low and overlapping micro-Dopplers. Similarly, the spatial resolution of the human in this perspective is also poor as seen in the inset in Fig.4(a). As a result of the poor resolution in all three dimensions, the quality of the Doppler-enhanced image in Fig.4(c) at $4.48s$ is quite poor. Next we consider the second radar orientation when the radar aperture is parallel to the direction of translation motion of the human with the aperture centered at $[-1, 1, 5]m$. In this orientation, the spatial resolution seen in the frontal perspective of the human is much improved as seen in the inset in Fig.4(a). Likewise, the micro-Dopplers are reasonably well resolved in the spectrogram in Fig.4(d) at $4.48s$. As a result, we are able to obtain a Doppler-enhanced frontal radar image in Fig.4(e) that bears reasonable qualitative resemblance to the frontal perspective.

IV. Conclusion

Frontal radar images of complex human motions can be generated with limited sized apertures at low carrier frequencies (below X band) by three-dimensional Fourier processing along Doppler, azimuth and elevation. Radar operators may find these images easier to interpret when compared to top view images of humans since frontal images resemble human perspectives. The quality of the radar images is a function of the range, orientation and Doppler of the target with respect to the radar.

Acknowledgment

This work is supported by the DST Inspire Faculty Fellowship granted by the Department of Science and Technology, Govt. of India.

References

[1] F. Ahmad, M. G. Amin, and S. A. Kassam, "Synthetic aperture beamformer for imaging through a dielectric wall," *Aerospace and Electronic Systems, IEEE Transactions on*, vol. 41, no. 1, pp. 271–283, 2005.

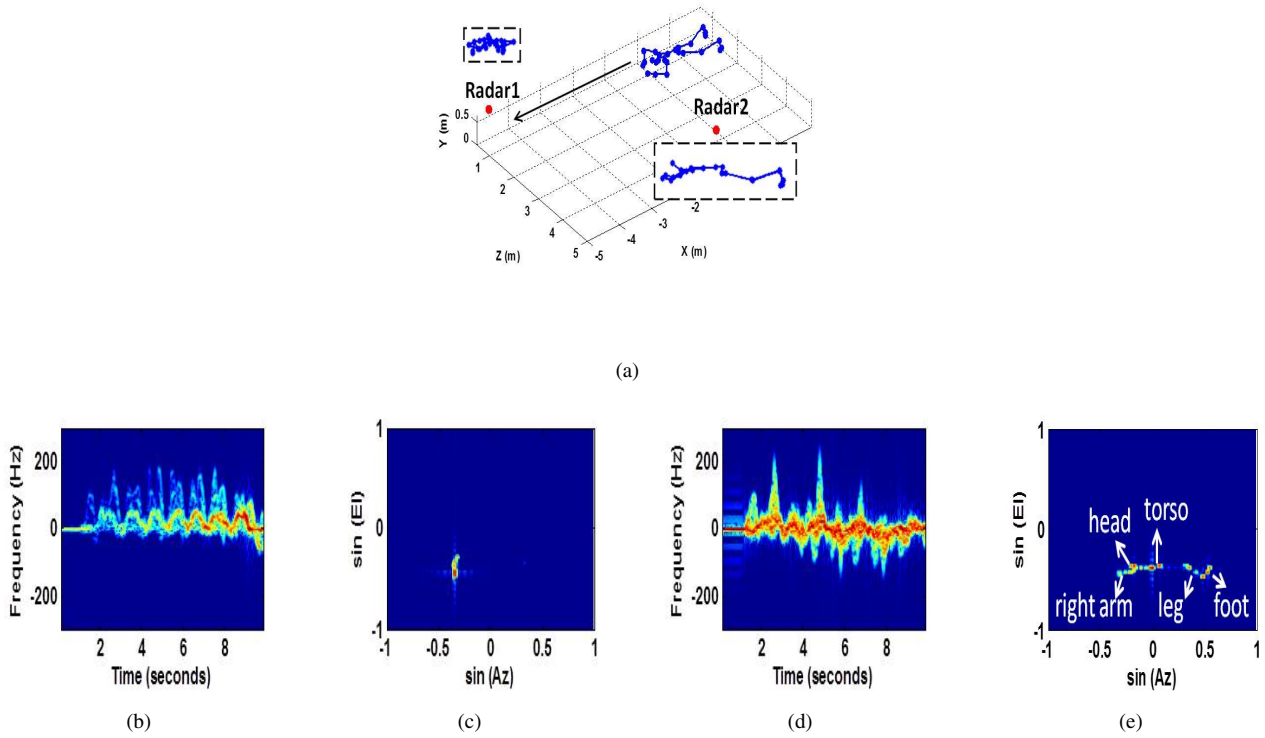

(a) (b) (c) (d) (e)

Fig. 4. (a) Animation model of a crawling human the two radar configurations: Radar1 corresponds to an aperture perpendicular to translational motion; Radar2 corresponds to an aperture parallel to the translational motion. (b) and (d) are Doppler spectrograms generated from time-domain data from a single sensor element; (c) and (e) are Doppler-enhanced frontal images of the human generated by three-dimensional Fourier processing - for Radar1 and Radar2 respectively.

[2] A. Yarovoy, L. Ligthart, J. Matuzas, and B. Levitas, "Uwb radar for human being detection," *Aerospace and Electronic Systems Magazine, IEEE*, vol. 21, no. 3, pp. 10–14, 2006.

[3] A. Lin and H. Ling, "Doppler and direction-of-arrival (ddoa) radar for multiple-mover sensing," *IEEE transactions on aerospace and electronic systems*, vol. 43, no. 4, pp. 1496–1509, 2007.

[4] J. Sachs, M. Aftanas, S. Crabbe, M. Drutarovsky, R. Klukas, D. Kocur, T. Nguyen, P. Peyerl, J. Rovnakova, and E. Zaikov, "Detection and tracking of moving or trapped people hidden by obstacles using ultra-wideband pseudo-noise radar," in *Radar Conference, 2008. EuRAD 2008. European*. IEEE, 2008, pp. 408–411.

[5] V. Chen, G. Smith, K. Woodbridge, and C. Baker, *Through-the-wall radar imaging*. CRC press, 2010, no. 15.

[6] M. G. Amin, *Through-the-wall radar imaging*. CRC press, 2011.

[7] I. Bilik, J. Tabrikian, and A. Cohen, "Gmm-based target classification for ground surveillance doppler radar," *Aerospace and Electronic Systems, IEEE Transactions on*, vol. 42, no. 1, pp. 267–278, 2006.

[8] G. E. Smith, K. Woodbridge, and C. J. Baker, "Template based micro-doppler signature classification," in *High Resolution Imaging and Target Classification, 2006. The Institution of Engineering and Technology Seminar on*. IET, 2006, pp. 127–144.

[9] T. Thayaparan, S. Abrol, E. Riseborough, L. Stankovic, D. Lamothe, and G. Duff, "Analysis of radar micro-doppler signatures from experimental helicopter and human data," *IET Radar, Sonar & Navigation*, vol. 1, no. 4, pp. 289–299, 2007.

[10] N. Maaref, P. Millot, C. Pichot, and O. Picon, "A study of uwb fm-cw radar for the detection of human beings in motion inside a building," *Geoscience and Remote Sensing, IEEE Transactions on*, vol. 47, no. 5, pp. 1297–1300, 2009.

[11] Y. Kim and H. Ling, "Human activity classification based on micro-doppler signatures using a support vector machine," *Geoscience and Remote Sensing, IEEE Transactions on*, vol. 47, no. 5, pp. 1328–1337, 2009.

[12] J. Bryan, J. Kwon, N. Lee, and Y. Kim, "Application of ultra-wide band radar for classification of human activities," *IET Radar, Sonar & Navigation*, vol. 6, no. 3, pp. 172–179, 2012.

[13] A. Lin and H. Ling, "Frontal imaging of human using three-element doppler and direction-of-arrival radar," *Electronics Letters*, vol. 42, no. 11, pp. 660–661, 2006.

[14] S. S. Ram and A. Majumdar, "High resolution radar imaging of moving humans using doppler processing and compressed sensing," *Aerospace and Electronic Systems, IEEE Transactions on*, accepted for publication.

[15] S. S. Ram and H. Ling, "Simulation of human microdopplers using computer animation data," in *Radar Conference, 2008. RADAR'08. IEEE*. IEEE, 2008, pp. 1–6.